# REPORT DOCUMENTATION PAGE

1

Form Approved OMB NO. 0704-0188



| 1. REPORT DATE (DD-MM-YYYY) | 2. REPORT TYPE | 3. DATES COVERED (From - To) |
|---|---|---|
| 29-08-2014 | Conference Proceeding | - |

**4. TITLE AND SUBTITLE**
An Unsteady Preconditioning Scheme Based on Convective-Upwind Split-Pressure (CUSP) Artificial Dissipation

**5a. CONTRACT NUMBER**
W911NF-12-1-0008

**5b. GRANT NUMBER**

**5c. PROGRAM ELEMENT NUMBER**
622307

**6. AUTHORS**
David Folkner, Aaron Katz, Venke Sankaran

**5d. PROJECT NUMBER**

**5e. TASK NUMBER**

**5f. WORK UNIT NUMBER**

**7. PERFORMING ORGANIZATION NAMES AND ADDRESSES**
Utah State University
1415 Old Main Hill - Room 64

Logan, UT 84322 -1415

**8. PERFORMING ORGANIZATION REPORT NUMBER**

**9. SPONSORING/MONITORING AGENCY NAME(S) AND ADDRESS (ES)**
U.S. Army Research Office
P.O. Box 12211
Research Triangle Park, NC 27709-2211

**10. SPONSOR/MONITOR'S ACRONYM(S)**
ARO

**11. SPONSOR/MONITOR'S REPORT NUMBER(S)**
60390-EG.30

**12. DISTRIBUTION AVAILIBILITY STATEMENT**
Approved for public release; distribution is unlimited.

**13. SUPPLEMENTARY NOTES**
The views, opinions and/or findings contained in this report are those of the author(s) and should not contrued as an official Department of the Army position, policy or decision, unless so designated by other documentation.

**14. ABSTRACT**
Obtaining accurate computational results for unsteady low-Mach number flows presents significant challenges for numerical schemes. In this work, we present a novel preconditioning scheme designed to provide good conditioning for these flows for all Strouhal numbers. The scheme is based on the convective-upwind split-pressure (CUSP) scheme which naturally facilitates the proper scaling of velocity and pressure dissipation terms for unsteady low-Mach number flows. Unlike traditional matrix dissipation schemes, the preconditioned CUSP formulation provides scaler-like efficiency and simplicity. Several test cases are presented for steady, unsteady, convection-dominated

**15. SUBJECT TERMS**
preconditioning, unsteady flows, CUSP

| 16. SECURITY CLASSIFICATION OF: | | | 17. LIMITATION OF ABSTRACT | 15. NUMBER OF PAGES | 19a. NAME OF RESPONSIBLE PERSON |
|---|---|---|---|---|---|
| a. REPORT | b. ABSTRACT | c. THIS PAGE | | | Aaron Katz |
| UU | UU | UU | UU | | 19b. TELEPHONE NUMBER 435-797-7021 |

**Report Title**

An Unsteady Preconditioning Scheme Based on Convective-Upwind Split-Pressure (CUSP) Artificial Dissipation


**ABSTRACT**

Obtaining accurate computational results for unsteady low-Mach number flows presents significant challenges for numerical schemes. In this work, we present a novel preconditioning scheme designed to provide good conditioning for these flows for all Strouhal numbers. The scheme is based on the convective-upwind split-pressure (CUSP) scheme which naturally facilitates the proper scaling of velocity and pressure dissipation terms for unsteady low-Mach number flows. Unlike traditional matrix dissipation schemes, the preconditioned CUSP formulation provides scalar-like efficiency and simplicity. Several test cases are presented for steady, unsteady, convection-dominated, and acoustic- dominated flows that demonstrate significant improvements in accuracy and convergence rate over traditional preconditioning schemes for a wide range of flow conditions.



**Conference Name:** AIAA SciTech 2014

**Conference Date:** January 07, 2014

# An Unsteady Preconditioning Scheme Based on Convective-Upwind Split-Pressure (CUSP) Artificial Dissipation*

David Folkner,† Aaron Katz,‡
*Department of Mechanical and Aerospace Engineering, Utah State University, Logan, UT 84322*

Venke Sankaran§
*Rocket Propulsion Division, AFRL, Edwards AFB, CA 93524*

**Obtaining accurate computational results for unsteady low-Mach number flows presents significant challenges for numerical schemes. In this work, we present a novel preconditioning scheme designed to provide good conditioning for these flows for all Strouhal numbers. The scheme is based on the convective-upwind split-pressure (CUSP) scheme which naturally facilitates the proper scaling of velocity and pressure dissipation terms for unsteady low-Mach number flows. Unlike traditional matrix dissipation schemes, the preconditioned CUSP formulation provides scalar-like efficiency and simplicity. Several test cases are presented for steady, unsteady, convection-dominated, and acoustic-dominated flows that demonstrate significant improvements in accuracy and convergence rate over traditional preconditioning schemes for a wide range of flow conditions.**

## I. Introduction

Low Mach number flows present significant challenges to compressible computational fluid dynamics (CFD) algorithms in terms of convergence rate and accuracy. Unlike transonic flows, low speed flows exhibit widely varying particle and acoustic speeds, which have a negative impact on convergence rate. Because pseudo-time scales are computed based on the fastest (acoustic) characteristic speeds, errors propagating at much lower particle velocities take much longer to convect out of the domain. For pseudo-time approaches that rely in part on convection of errors to reach steady state, this can have a disastrous effect on convergence rate. Even if steady state is obtained for low Mach number flows (after many iterations), the results may prove inaccurate due to improper scaling of the artificial dissipation operator. This has been observed in practice and in theory through asymptotic analysis of the Navier-Stokes equations.

Preconditioning schemes have proven highly successful at improving accuracy and convergence for steady low Mach number flow computations, as well as higher Mach number flows exhibiting regions of low speed flow, such as boundary layers or stagnation points. By simultaneously modifying and wave speeds in pseudo-time as well as artificial dissipation scaling, preconditioning can extend favorable properties observed for transonic flows to low Mach number regimes. Improvements in accuracy and convergence can be dramatic, as demonstrated by many researchers [1, 2, 3, 4]. Furthermore, preconditioning facilitates the use of a variety of state equations necessary for real gas effects, multiphase flows, and combustion [5].

While preconditioning has proven highly successful for steady flows, challenges remain to extend preconditioning to unsteady flows for which propagation of vortical and acoustic features in physical time becomes a complicating factor. For these flows, it is important to consider the effect of preconditioning on pressure and velocity dissipation effects separately. At low Mach numbers, classical "steady" preconditioning methods increase the pressure dissipation, while reducing the velocity and temperature field dissipation, thereby insuring well-conditioned accuracy at all speeds. The situation gets murkier for unsteady flows. Here, one must distinguish between vortex propagation and acoustic wave propagation. For the former case, the so-called "low Strouhal" limit, the above observation remains true and the steady preconditioning formulation maintains optimal accuracy at all speeds. For acoustic propagation, referred to as the "high Strouhal" limit, steady preconditioning results in overly dissipative pressure dissipation, while the velocity and temperature fields are optimally handled. On the other hand, when no preconditioning is used, the pressure field is optimally handled, while the velocity and temperature fields become overly dissipative.

*Distribution Statement A: Approved for public release; distribution is unlimited. PA Clearance Number 13322.
†Graduate Student, Member AIAA.
‡Assistant Professor, Member AIAA.
§Senior Scientist, Member AIAA.

In order to address the dilemma for low-Mach unsteady flows in the acoustic limit, blended dissipation schemes were introduced by Xia et al. [6] for the scalar dissipation case and by Potsdam et al. [7] for the matrix dissipation case. Further work on unsteady preconditioning was performed by Hosangadi et al.[8]. In the case of matrix dissipation, separate treatment of pressure and velocity becomes difficult due to the simultaneous coupling of these terms. Nevertheless, Potsdam et al. [7] demonstrated that is it still possible.

The selection of different scaling for the pressure and velocity diffusion terms is perhaps more readily accomplished via the AUSM schemes of Liou and Steffen[9, 10, 11], or the convective-upwind split-pressure (CUSP) scheme of Jameson[12, 13], since they provide distinct formulations for these terms. For the steady case, Liou provides a modification to extend AUSM for all speeds, which he terms AUSM$^+$-up[11]. Similarly, Zha et al.[14, 15] provides a modification to CUSP suitable for low Mach number steady flows, although it appears that this formulation more closely resembles the AUSM framework.

The goal of this work is to explore CUSP-based preconditioning schemes suitable for all speed steady and unsteady flows. This is accomplished via the addition of properly scaled pressure diffusion to the original CUSP scheme of Jameson. Flows at the high and low Strouhal limits are explored in terms of accuracy and convergence. Furthermore, steady cases are examined to verify the spatial order of accuracy. We find that the preconditioned CUSP scheme provides accurate results and good convergence at all flow conditions tested. Moreover, the scheme retains the simplicity and economy of the original CUSP formulation.

The paper is organized as follows: First, a general preconditioning framework is outlined based on primitive variables. Modifications for steady and unsteady flows are given. Next, the formulation of the new preconditioned CUSP scheme is given. Following this, results are presented for steady and unsteady flows for convective and acoustic dominated cases at low and high Strouhal numbers. Finally preliminary results are given along with plans for future work.

## II. General Preconditioning Framework

The purpose of this section is to formulate a general framework encompassing most preconditioning schemes proposed in the literature. Preconditioning schemes have been proposed by many researchers to improve convergence and accuracy for compressible flows using a pseudo-time solution procedure [1, 2, 3, 4]. We present the framework in two-dimensions for simplicity, but extensions to three-dimensions follow readily. In subsequent sections we use this framework to describe the new preconditioned CUSP scheme.

Following the general notation of Merkle [5], the steady inviscid Euler equations are

$$\frac{\partial Q}{\partial \tau} + \frac{\partial F}{\partial x} + \frac{\partial G}{\partial y} = 0, \tag{1}$$

where

$$Q = \begin{Bmatrix} \rho \\ \rho u \\ \rho v \\ \rho E \end{Bmatrix}, \quad F = \begin{Bmatrix} \rho u \\ \rho u^2 + p \\ \rho uv \\ \rho u h^0 \end{Bmatrix}, \quad G = \begin{Bmatrix} \rho v \\ \rho uv \\ \rho v^2 + p \\ \rho v h^0 \end{Bmatrix}. \tag{2}$$

Here, $Q$ represents the vector of conserved variables, and $F$ and $G$ represent the inviscid fluxes in the $x$- and $y$-directions respectively. The preconditioning method outlined by Merkle involves a conversion from conserved variables to primitive variables,

$$Q_v = \begin{Bmatrix} p \\ u \\ v \\ T \end{Bmatrix}, \tag{3}$$

where $Q_v$ is the vector of primitive variables. The use of primitive variables generally simplifies many aspects of the present derivation. More importantly, primitive variables greatly simplify the implementation of a variety of equations of state and real gas effects. For example, enthalpy is often tabulated as a function of temperature for many gases. With conservative variables it is necessary to iteratively find temperature from enthalpy. However, since temperature is available directly from the primitive variables, the enthalpy can be extracted with little effort in this approach.

Conversion from conserved variables to primitive variables is facilitated via the Jacobian matrix,

$$\Gamma \equiv \frac{\partial Q}{\partial Q_v} = \begin{bmatrix} \rho_p & 0 & 0 & \rho_T \\ u\rho_p & \rho & 0 & u\rho_T \\ v\rho_p & 0 & \rho & v\rho_T \\ h^0\rho_p + \rho h_p - 1 & \rho u & \rho v & h^0\rho_T + \rho h_T \end{bmatrix}, \tag{4}$$

where subscripts $p$ and $T$ denote partial differentiation (e.g. $\rho_p = \partial\rho/\partial p$). Here the equation of state is formulated as

$$\rho = \rho(p, T), \quad h = h(p, T). \tag{5}$$

Finite volume discretizations of Equation 1 involve the computation of directed fluxes at volume faces, $\mathcal{F} = \boldsymbol{A} \cdot \boldsymbol{F}$, with area vector, $\boldsymbol{A} = (A_x, A_y)^T$. The wave speeds of the discrete scheme in pseudo-time are the eigenvalues of the product of $\Gamma^{-1}$ and the directed flux Jacobian with respect to the primitive variables, $\mathcal{A} = \partial\mathcal{F}/\partial Q_v$:

$$\lambda\left(\Gamma^{-1}\mathcal{A}\right) = |\boldsymbol{A}|(u_n, u_n, u_n \pm c), \tag{6}$$

with area magnitude $|\boldsymbol{A}| = \sqrt{A_x^2 + A_y^2}$, normal velocity $u_n = \boldsymbol{u} \cdot \boldsymbol{n}$, and unit normal, $\boldsymbol{n} = \boldsymbol{A}/|\boldsymbol{A}|$. Here $c$ is the sound speed, defined for general equations of state as,

$$c^2 = \frac{\rho h_T}{\rho h_T \rho_p + \rho_T(1 - \rho h_p)}. \tag{7}$$

Large disparities in the wave speeds of Equation 6 result in poor convergence. The goal of a preconditioner is to reduce the wave speed disparities. In this approach, the matrix $\Gamma$, arising in the pseudo-time derivative is replaced by a preconditioning matrix, $\Gamma_p$, in the governing equations:

$$\Gamma\frac{\partial Q_v}{\partial \tau} + \frac{\partial F}{\partial x} + \frac{\partial G}{\partial y} = 0 \quad \longrightarrow \quad \Gamma_p\frac{\partial Q_v}{\partial \tau} + \frac{\partial F}{\partial x} + \frac{\partial G}{\partial y} = 0$$

The matrix $\Gamma_p$ is selected such that the eigenvalues of $\Gamma^{-1}\mathcal{A}$ are the same order of magnitude. This is accomplished by defining $\Gamma_p$ as,

$$\Gamma_p = \begin{bmatrix} \rho'_p & 0 & 0 & \rho_T \\ u\rho'_p & \rho & 0 & u\rho_T \\ v\rho'_p & 0 & \rho & v\rho_T \\ h^0\rho'_p + \rho h_p - 1 & \rho u & \rho v & h^0\rho_T + \rho h_T \end{bmatrix} \tag{8}$$

It is observed that $\Gamma_p$ is identical to $\Gamma$, except that a new term, $\rho'_p$, replaces $\rho_p$. In terms of $\rho'_p$, the eigenvalues of the preconditioned system become

$$\lambda\left(\Gamma^{-1}\mathcal{A}\right) = |\boldsymbol{A}|\left(u_n, u_n, \frac{1}{2}\left[u_n\left(1 + \frac{d}{d'}\right) \pm \sqrt{u_n^2\left(1 - \frac{d}{d'}\right)^2 + 4\frac{\rho h_t}{d'}}\right]\right), \tag{9}$$

where

$$\begin{aligned} d &= \rho h_T \rho_p + \rho_T(1 - \rho h_p) \\ d' &= \rho h_T \rho'_p + \rho_T(1 - \rho h_p). \end{aligned} \tag{10}$$

The selection of $\rho'_p$ is guided by the principle that a good preconditioner should force the acoustic wave speeds to be the same order of magnitude as the particle speeds. Following Sankaran [1] and Merkle [5], the acoustic waves of the preconditioned system in Equation involve a "preconditioned sound speed," $V_p$,

$$V_p^2 \equiv \frac{\rho h_t}{d'} \tag{11}$$

If one selects $V_p$ to be the same order of magnitude as the particle wave speeds, the goal of preconditioning is achieved. Once the preconditioned sound speed is selected, Equation 11 provides a definition of $\rho'_p$ in terms of $V_p$:

$$\rho'_p = \frac{1}{V_p^2} - \frac{\rho_T(1 - \rho h_p)}{\rho h_T} \tag{12}$$

In this manner, the properties of the preconditioner depend primarily on what one chooses for $V_p$. The following sections provide methods to determine the preconditioned sound speed for steady and unsteady flows.

### A. Steady Preconditioning

For steady problems, wave information propagates at convective and acoustic speeds in pseudo-time only. In this case, the preconditioned sound speed is set to the magnitude of the particle wave speed,

$$V_p^s = \sqrt{u^2 + v^2}. \tag{13}$$

Here the superscript "s" denotes that this definition is for steady flows. At low speeds, this definition of $V_p^s$ improves convergence and adjusts the scaling of the artificial dissipation operator [1]. For supersonic flows, however, preconditioning is unnecessary, and accuracy actually suffers [1] when the preconditioned sound speed is larger than the physical sound speed. To limit the preconditioned sound speed for high speed steady flows, we choose,

$$V_p^s = \min\left(\sqrt{u^2 + v^2}, c\right) \tag{14}$$

In supersonic regimes, Equation 14 sets the preconditioned sound speed to the physical sound speed. This reverts the eigenvalues to their non-preconditioned form and turns off the preconditioner.

### B. Unsteady Preconditioning

For unsteady problems, information propagates in pseudo-time and physical time. As the relevant physical time scale, $\Delta t$, becomes small, physical acoustic waves are of primary consideration. Hosangadi, et al. [8] showed that modification of the preconditioned sound speed from the physical value in this case can cause convergence and accuracy degradation. In this discussion, we refer to flows with small physical time scales, $\Delta t$, has high Strouhal number flows, where the Strouhal number,

$$Str = \frac{L}{\pi \Delta t \sqrt{u^2 + v^2}}, \tag{15}$$

represents a characteristic non-dimensional frequency. High Strouhal number flows are dominated by acoustic wave action. Flows with large physical time scales are low Strouhal number flows. Taken in the limit, these flows revert to steady flows.

In this light, a good unsteady preconditioner should turn off for high Strouhal number flows to allow proper capturing of the physical acoustic waves, and revert to the steady formulation as the Strouhal number becomes small. This is accomplished by defining the preconditioned sound speed to be

$$V_p^u = \min\left[\max\left(\sqrt{u^2 + v^2}, Str\sqrt{u^2 + v^2}\right), c\right], \tag{16}$$

where the superscript "u" denotes that this definition is for steady flows. The addition of the Strouhal number in this manner allows for a smooth transition between steady and unsteady (acoustically driven) flows.

In both steady and unsteady problems, proper treatment of stagnation points with preconditioning is critical. Stagnation points are common in external aerodynamics at leading and trailing edges of wings. In these regions, the particle velocity approaches zero and the definitions of $V_p^s$ and $V_p^u$ become ill-posed. This is often overcome for external flows by specifying a minimum velocity scale proportional to the free stream velocity. In stagnation regions, this minimum velocity scale is used instead of the particle velocity which may approach zero. For other types of flows, such as internal flows, a free stream value is not readily available and using the particle velocity from nearby cells as a reference often works well in practice. For the cases considered in this work, the free stream specification method is used.

## III. Preconditioned CUSP Scheme

The previous section discussed preconditioning primarily as a convergence acceleration tool. The other critical aspect of preconditioning is its effect on accuracy through the scaling of numerical dissipation operators needed for stability of non-linear systems of equations, such as the Euler and Navier-Stokes equations. This can be seen by examining the effect of preconditioning on a finite volume numerical flux with matrix dissipation,

$$\hat{\mathcal{F}} = \frac{1}{2}\left(\mathcal{F}(Q_L) + \mathcal{F}(Q_R)\right) - \Gamma_p \left|\Gamma_p^{-1}\mathcal{A}_v\right| \left(Q_{vR} - Q_{vL}\right). \tag{17}$$

Extensive research has been performed using matrix dissipation with both steady and unsteady preconditioners. Hosangadi et al. [8] showed through asymptotic analysis the general behavior for these schemes. A table showing the effects of Strouhal number and Mach number on the accuracy of the dissipation for the pressure and velocity fields is shown in Table 1.

Steady Low Mach Number Limit

| | Pressure Field | Velocity Field |
|---|---|---|
| No Preconditioning | O(M) | O(1/M) |
| Steady Preconditioning | O(1) | O(1) |

Unsteady Low Mach/ Low-Str Number Limit

| | Pressure Field | Velocity Field |
|---|---|---|
| No Preconditioning | O(M) | O(1/M) |
| Steady Preconditioning | O(1) | O(1) |
| Unsteady Preconditioning | O(1) | O(1) |

Unsteady Low Mach/ High-Str Number Limit

| | Pressure Field | Velocity Field |
|---|---|---|
| No Preconditioning | O(1) | O(1/M) |
| Steady Preconditioning | O(Str) | O(1) |
| Unsteady Preconditioning | O(1) | O(1/M) |

**Table 1. Preconditioning effects on artificial dissipation scaling [8].**

From Table 1, it is clear that matrix dissipation is sufficient for steady or low Strouhal number problems. However, matrix dissipation accuracy suffers when the Strouhal number is high and Mach number is low. In these cases, steady preconditioning is capable of resolving velocity fields, but pressure fields suffer. The opposite is true of the unsteady preconditioner. To remedy the situation, Potsdam [7] created a "blended matrix scheme" that uses selection matrices to combine the pressure fields of the unsteady preconditioner and the velocity fields of the steady preconditioner.

As an alternate option, we consider the convective-upwind split-pressure (CUSP) framework proposed by Jameson [12]. The CUSP scheme is nearly as inexpensive as scalar dissipation but retains comparable shock capturing characteristics. Furthermore, it naturally splits convective and pressure effects, which proves advantageous in a preconditioning context. The CUSP scheme is given by,

$$D(Q_R, Q_L) = \frac{1}{2}\alpha^* |\boldsymbol{A}| \Delta Q + \frac{1}{2}\beta \left(\mathcal{F}(Q_R) - \mathcal{F}(Q_L)\right) \tag{18}$$

where $\Delta Q = Q_R - Q_L$. Equivalently the CUSP scheme may be expressed as,

$$D(Q_R, Q_L) = \frac{1}{2}\alpha |\boldsymbol{A}| c \Delta Q + \frac{1}{2}\beta |\boldsymbol{A}| \overline{Q} \Delta u_n + \frac{1}{2}\beta \Delta \mathcal{F}_p \tag{19}$$

where

$$\alpha c = \alpha^* c + \beta \overline{u}_n, \quad \mathcal{F}_p = \begin{Bmatrix} 0 \\ A_x p \\ A_y p \\ |\boldsymbol{A}| u_n p \end{Bmatrix}. \tag{20}$$

Here, an overbar refers to the arithmetic average of right and left states.

In the CUSP scheme, $\alpha$ and $\beta$ are chosen to give proper upwinding characteristics in subsonic and supersonic regimes, while maintaining good shock capturing for transonic regions:

$$\alpha = |M_n| \tag{21}$$

$$\beta = \begin{cases} \max(0, 2M_n - 1) & \text{if } 0 \le M_n \le 1 \\ -\max(0, 2M_n + 1) & \text{if } -1 \le M_n \le 0 \\ \text{sign}(M_n) & \text{if } |M_n| \ge 1 \end{cases} \tag{22}$$

Here, $M_n = u_n/c$ is the local directional Mach number.

Unfortunately, the original CUSP scheme above encounters similar problems as the matrix scheme at low Mach numbers. In order to determine modifications suitable for preconditioning, we note that Liou et. al. [11] observed similar difficulties with AUSM. To solve the issue in AUSM, Liou introduced two new forms of dissipation into the AUSM scheme: additional pressure dissipation for the interfacial Mach number and additional velocity diffusion to the pressure terms. While the addition of pressure dissipation has been used extensively in the literature [14, 15, 8]

with much success, the effects of velocity dissipation are less clear. Since the focus is on low speed flows, velocity dissipation is omitted.

Following the work of Liou, additional pressure diffusion may be added to the CUSP scheme in the form

$$D_p(Q_R, Q_L) = \gamma |\boldsymbol{A}| \overline{\tilde{c}} \overline{Q} \Delta p \tag{23}$$

where

$$\gamma = \frac{K_p}{f_a} \frac{\max(1 - \alpha \overline{M_e}^2, 0)}{\overline{\rho c}^2}, \tag{24}$$

$$f_a = M_o(2 - M_o), \quad M_o^2 = \min(\max(\overline{M_e}^2, \overline{M_e}^2 Str^2), 1), \tag{25}$$

$$M_e = \frac{\sqrt{u^2 + v^2}}{c}. \tag{26}$$

Here, $K_p$ is taken as 0.25 in this work. The final modified CUSP scheme is then,

$$D(Q_R, Q_L) = \frac{1}{2}\alpha |\boldsymbol{A}| c \Delta Q + \frac{1}{2}\beta |\boldsymbol{A}| \overline{Q} \Delta u_n + \frac{1}{2}\beta \Delta \mathcal{F}_p + D_p(Q_R, Q_L) \tag{27}$$

While CUSP presents advantages in terms of efficiency over the matrix scheme, its differentiation does not naturally lead do a diagonally dominant left-hand-side matrix, which causes stability problems for implicit Gauss-Seidel schemes. For this reason, matrix dissipation is always used on the left hand side in this work.

# IV. Results

In this section, we present steady and unsteady results to assess the new preconditioned CUSP scheme. In all cases we compare with established matrix dissipation schemes. First, we verify that all preconditioning schemes tested have been implemented properly via the method of manufacture solutions (MMS). A steady state airfoil is also analyzed for validation purposes. Second, in order to assess the accuracy for low Strouhal and low Mach number unsteady flows, we compute results for an inviscid propagating vortex. Finally, flow in a one-dimensional pipe with high-frequency (in time) oscillating back pressure is computed. The high pressure oscillation generates acoustic waves at high Strouhal numbers. The results from Table 1 are validated using matrix dissipation and compared to the new CUSP algorithm described by this work. Convergence history of these cases is provided to illustrate the effect of low-speed preconditioning on temporal convergence.

## A. Verification and Validation for Steady Flows

Verification provides a robust way of confirming numeric accuracy and code implementation. It is beneficial to use MMS verification any time a new scheme is being introduced. This simple check was performed in Fig. 1 using steady state MMS. The different lines and symbols found throughout Fig. 1 are described by Table 2.

The MMS verification is able to show that for all quantities and methods, the output is second order accurate and behaves properly. It is interesting to observe that although all lines are second order accurate, the accuracy is clearly changing. This could be due to a number of factors. Regardless of whether the RHS is using CUSP or matrix dissipation, the LHS requires the use of the diagonally dominant matrix scheme. For the parameters of source terms chosen to define the MMS solution, the optimum preconditioned pressure additions of CUSP could be providing an excessive amount of dissipation.

| Symbol | Test Scenario |
|---|---|
| $R^N$ | matrix dissipation with No preconditioning |
| $R^S$ | matrix dissipation with Steady preconditioning |
| $C^N$ | CUSP dissipation with No preconditioning |
| $C^S$ | CUSP dissipation with Steady preconditioning |

**Table 2. List of test scenarios for Fig .1**

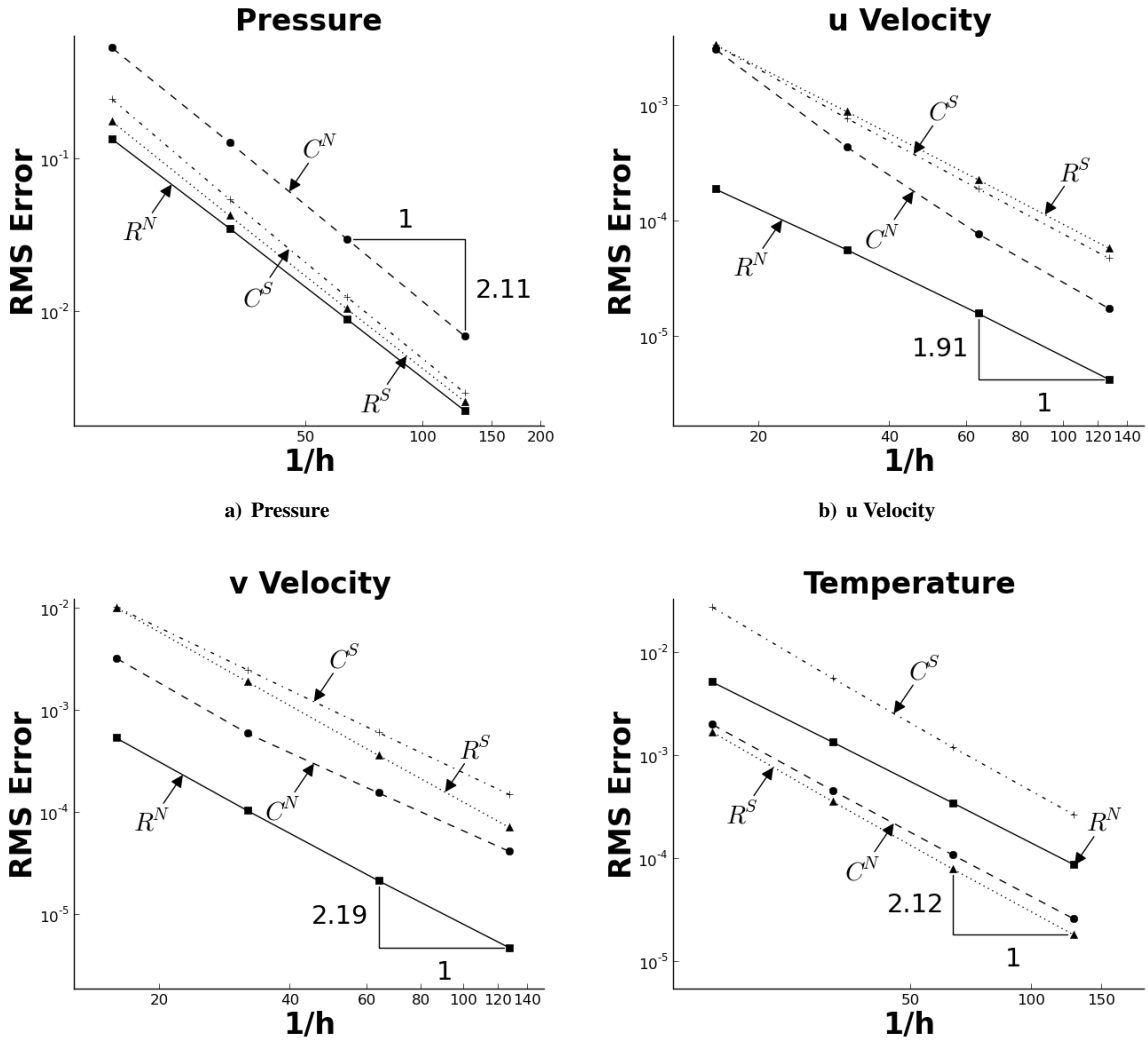


**a) Pressure** **b) u Velocity**

**c) v Velocity** **d) Temperature**

**Figure 1. Verification plots using steady state MMS for primitive variables $p$, $u$, $v$, and $T$ with a Mach number of 0.05. Symbols are defined by Table 2**

To get general validation of the dissipation schemes, a NACA 0012 airfoil was tested at a relatively low Mach number. Fig. 2 shows the pressure contours for a variety of cases. A free-stream cut-off velocity was specified for preconditioning at the stagnation point and is necessary for convergence. Fig. 2c shows the solution without preconditioning. The stagnation point is not captured in the detail as the two preconditioned cases found in Figs. 2a and 2b. Near the stagnation point, the particle velocity approaches zero. This creates a very large disparity in the wave speeds. Although the solution in the non-preconditioned case converges, it is possible for the overall convergence criteria to be reached where large errors are still propagating locally near the stagnation point. Local preconditioning aids in overall convergence, as well as the convergence at the stagnation point.

The iterations for each airfoil is also reported in Fig. 2. Without preconditioning, dramatic efficiency problems are seen. Implementation of CUSP slows down convergence slightly. This is generally attributed to the difference between the LHS and RHS in the implementation. This simple case highlights how preconditioning is able to increase the accuracy of the solution as well as aids in convergence.

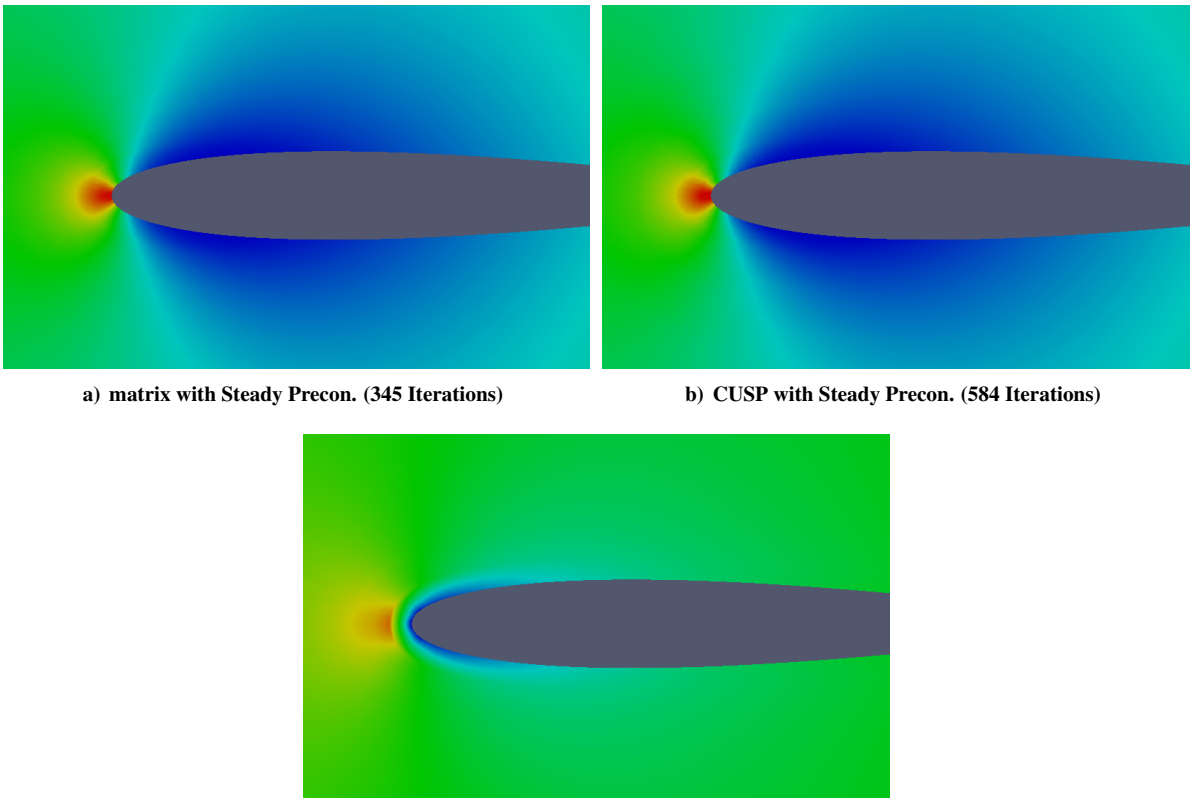

**a) matrix with Steady Precon. (345 Iterations)**

**b) CUSP with Steady Precon. (584 Iterations)**

**c) matrix without Precon. (2724 Iterations)**

**Figure 2. Pressure contours of a 2D NACA 0012 airfoil with free stream Mach number of 0.05 with no angle of attack.**

## B. Inviscid Propagating Vortex

Inviscid vortices are primarily velocity driven problems. Although a pressure field exists, pressures only respond to the velocity field. An inviscid propagating vortex is an unsteady problem, where some vortex travels at a free stream ($U_\infty$) velocity in time. Ideally, the vortex will maintain it's shape with time and simply translate through the domain. CFD discretization creates diffusion that will introduce errors into the solution. To test this phenomenon, a simple 2D vortex is used to initialize the domain. Unsteady time steps are used to allow the vortex to propagate across the domain. In this simplified case, it is assumed the free stream velocities only exist in the $x$ direction.

The vortex is initialized using several user defined parameters. $R$ is the radius of the vortex, $\beta$ is the strength of the vortex, and $x_c$ and $y_c$ are used to specify it's starting point. Fig. 3 shows a sample 2D initialization of the vorticity over a square domain. The following equations define how the vortex is initialized and assume an ideal gas equation of state.

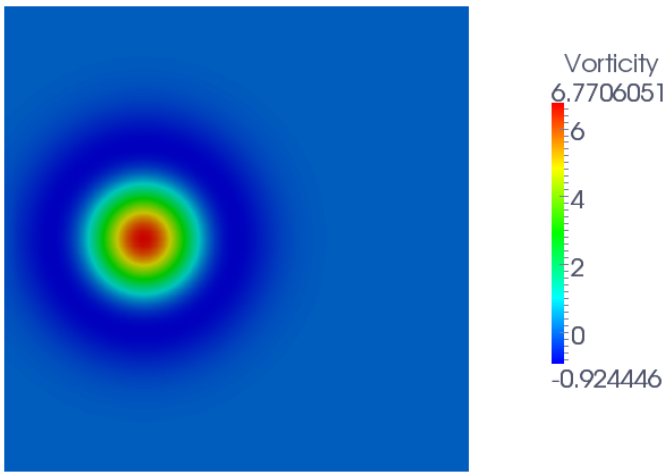


**Figure 3. Initial contour of vorticity on a 64 by 64 mesh.**

$$\begin{aligned} \delta u &= -U_\infty \beta \tfrac{y-y_c}{R} e^{-r^2/2} \\ \delta v &= U_\infty \beta \tfrac{x-x_c}{R} e^{-r^2/2} \\ \delta T &= 0.5(U_\infty \beta)^2 e^{-r^2}/c_p \end{aligned} \tag{28}$$

where

$$\begin{aligned} &u_0 = U_\infty + \delta u, \quad v_0 = \delta v, \quad T_0 = T_\infty - \delta T \\ &\rho_0 = \rho_\infty \left(\tfrac{T_0}{T_\infty}\right)^{\frac{1}{\gamma-1}}, \quad \rho_\infty = \tfrac{P_\infty}{R_{gas} T_\infty}, \quad P_0 = \rho_0 * R_{gas} T_0 \\ &r = \tfrac{\sqrt{(x-x_c)^2+(y-y_c)^2}}{R}, \quad U_\infty = M_\infty \sqrt{\gamma R_{gas} T_\infty} \end{aligned} \tag{29}$$

Due to the unsteady nature of the problem, the boundaries of the domain become difficult to enforce. The exact solution as a function of time was imposed on the boundaries. This may cause issues as the vortex enters or leaves the domain. To avoid this issue, boundaries were placed "far" from the edges of the vortex.

In the absence of viscous terms, the exact solution should allow the vortex to travel with no diffusion at the free stream velocity. The exact solution can be represented by the initialization equations from Eqs. 28 and 29 where the center is moving. The new center is found as,

$$x_c(t) = x_{c0} + U_\infty t, \quad y_c(t) = y_{c0} \tag{30}$$

At a given time, the exact vorticity can be found to be:

$$\omega = \frac{U_\infty \beta}{R} e^{-r^2/2}(2 - r^2) \tag{31}$$

For unsteady problems, selection of the physical time step is critical. It is important to choose a time step to capture the flow dynamics efficiently and correctly. The "CFL" number relates a velocity, time step, and cell width to help specify the time step.

$$CFL = \frac{\mathcal{U}dt}{dx} \tag{32}$$

where $\mathcal{U}$ is some velocity scale, $dx$ is typically taken as the average cell width and $dt$ is the physical time step. $\mathcal{U}$ can be chosen to be either the particle speed ($CFL_u$) or the acoustic speed ($CFL_c$). $CFL_u = 1$ allows the particles to move about 1 cell per time step, where $CFL_c = 1$ allows the physical acoustics do the same. These two situations are of current interest specifically how the new CUSP modification and preconditioners behave.

In order to validate the accuracy of Table 1, as well as the implementation of the preconditioners, matrix diffusion was tested. For this velocity driven case, Table 1 indicates that using no preconditioner and the unsteady preconditioner in the high Strouhal limit will yield reduced accuracy.

Fig. 4a shows the data for a "snapshot" of vorticity at some time after the vortex is allowed to translate down stream for various preconditioners. The vorticity is taken at the centerline. The steady preconditioner captures the vorticity (or velocity field) much better than the non-preconditioned case. The introduction of the Strouhal number in the unsteady case, works to "blend" the steady preconditioner to the un-preconditioned case. Here, the time step is large enough that the high Strouhal limit is not reached.

Fig. 4b shows the convergence of the psuedo-time terms at a given time step. The unsteady preconditioner outperforms the other schemes. By converging with fewer iterations, the unsteady preconditioner decreases the computation time required. Fig. 4b highlights just one of many time steps. As the number of time steps in a problem grows, this speed up becomes increasingly important. The results from Fig. 4 are consistent with those found in Hosangadi et. al. [8] and with Table 1.

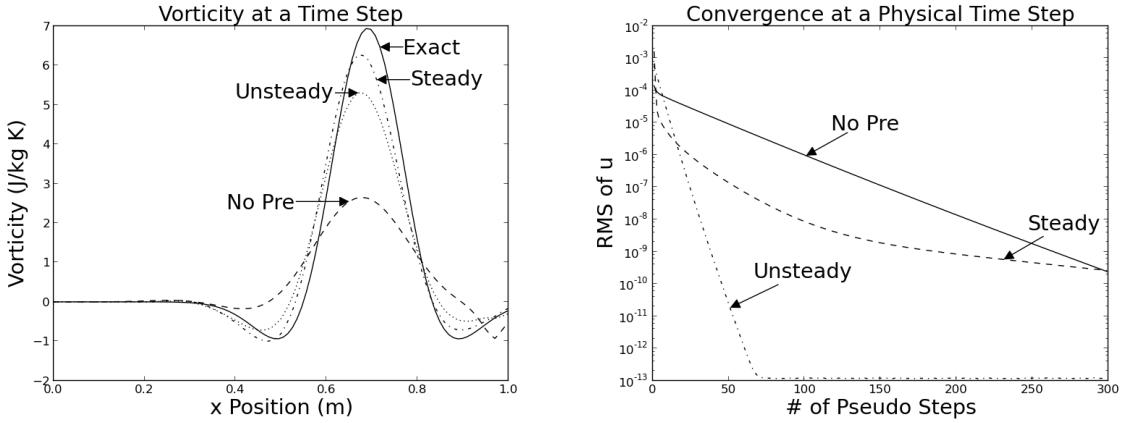


**a) Vorticity** **b) Convergence**

**Figure 4. Plots of propagating vortex with matrix diffusion on a square domain with a $CFL_u = 1$, $Str = 20.4$, $Mach = 0.005$, and 20 points across the vortex.**

To explore the effects of higher Strouhal numbers, the CFL number was lowered. Fig. 5 shows a similar case to Fig. 4, but with a $CFL_c = 1$ rather than $CFL_u = 1$. The reduction in the time step causes a dramatic increase to the Strouhal number. In this case, the unsteady preconditioner reduces to the un-preconditioned state, consistent with its definition. The vorticity plot found in Fig. 5a shows this behavior and highlights the unsteady preconditioners inability to accurately describe the velocity field at high Strouhal numbers. Again, Fig. 5b shows that the steady preconditioner suffers to efficiently converge in this highly unsteady case.

The unsteady preconditioning method is extremely effective at converging efficiently. When the time step is very small, it outperforms the steady preconditioner. As time steps grow, it is capable of reducing to the steady preconditioner. This process is shown by Fig. 4b. The convergence advantages of the unsteady preconditioner are offset in this scenario by the drop in velocity field accuracy. The desire to capitalize on the unsteady preconditioners superior convergence while not loosing accuracy is the main motivation behind the implementation of a preconditioned CUSP.

In order to showcase the effectiveness of CUSP, the cases in Figs. 4 and 5 were re-run using the newly modified CUSP diffusion algorithm. These results are found in Figs. 6 and 7.

Both Figs. 6a and 7a show accuracy improvements in the unsteady preconditioned case when compared to their matrix counter parts. In the low Mach number high Strouhal number limit, the modified CUSP is able to resolve

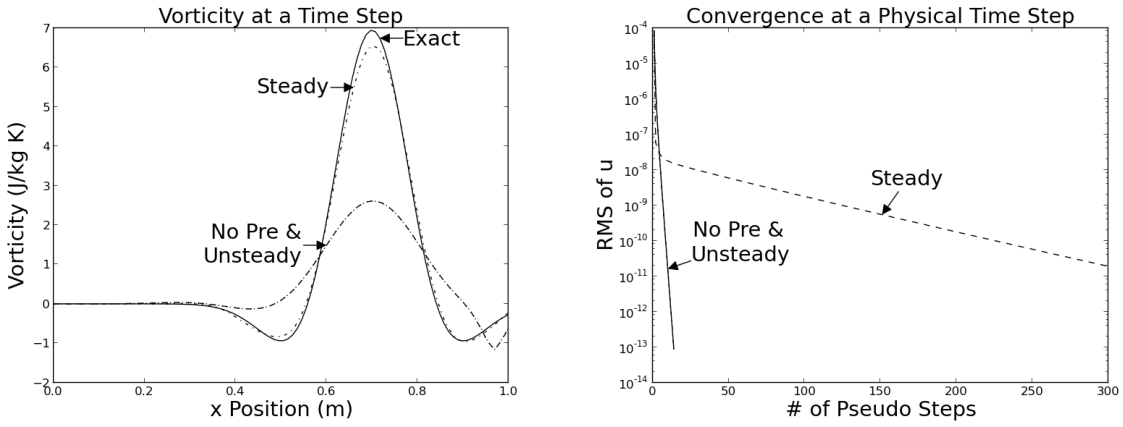


**a) Vorticity** **b) Convergence**

**Figure 5. Plots of propagating vortex with matrix diffusion on a square domain with a $CFL_c = 1$, $Str = 4076$, $Mach = 0.005$, and 20 points across the vortex.**

the unsteady issue that matrix dissipation exhibits. Similar to the airfoil in the previous section, CUSP shows a slight decrease in convergence when compared with matrix dissipation. This is most likely due to the LHS and RHS discrepancies.

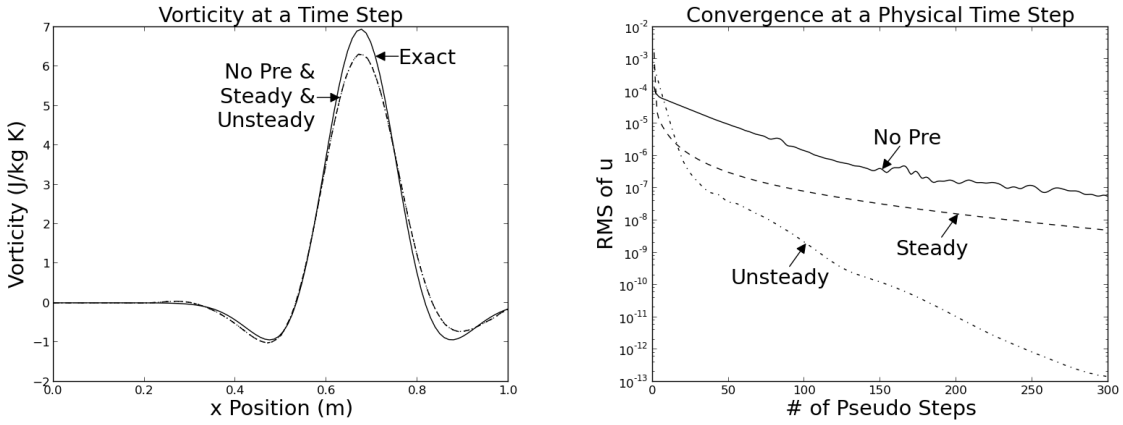


**a) Vorticity** **b) Convergence**

**Figure 6. Plots of propagating vortex with CUSP diffusion on a square domain with a $CFL_u = 1$, $Str = 20.4$, $Mach = 0.005$, and 20 points across the vortex.**

### C. Oscillating Back Pressure in a Pipe

The previous case highlighted the velocity field. In order to isolate the pressure field, a case was devised to purposefully introduce pressure waves as the driving factor. A simple 1D pipe was modeled using a 2D cell-centered code with uniform cells in the y-direction. Pressure on the outflow was oscillated sinusoidally in time to create pressure waves. This is represented by:

$$p_{x=L} = P_\infty(1 + \epsilon sin(wt)) \tag{33}$$

where $P_\infty$ is the free-stream pressure, $p_{x=L}$ is the outlet pressure, $w$ is the frequency that the pressure is driven, $t$ is the physical time, and $\epsilon$ is some scale factor.

The selection of $\epsilon$ was set so the overall pressure varied less than 1/2 of the dynamic pressure. This prevents the pressure oscillation from reversing the flow direction. It is noteworthy that 1/2 was chosen relatively arbitrarily. $\epsilon$ is

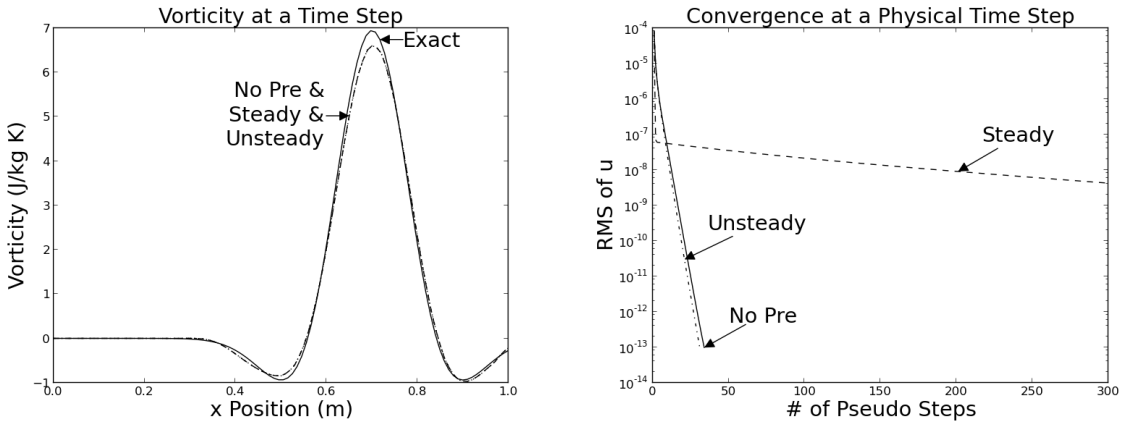


**a) Vorticity** **b) Convergence**

**Figure 7. Plots of propagating vortex with CUSP diffusion on a square domain with a $CFL_c = 1$, $Str = 4076$, $Mach = 0.005$, and 20 points across the vortex.**

defined below by:

$$\epsilon = 0.5\frac{0.5\rho_\infty u_\infty^2}{P_\infty} \tag{34}$$

Another dimensionless parameter is introduced that relates the frequency of oscillation, the length scale of the domain, and the initial flow velocity. The length scale (length of the pipe $L$) for this problem was set to one. This parameter ($\Omega$) is used to set the frequency of oscillation.

$$\Omega = \frac{wL}{u_0} \tag{35}$$

The boundary conditions for the inlet of the pipe warrant discussion. It is necessary to fix enough of the state to close the problem, while still allowing the outflow pressure to propagate. One method is to use non-reflecting Riemann invariants. Here, stagnation pressure and enthalpy were fixed at the inlet. These allow the pressure to propagate out the inlet, but do exhibit some reflective behavior. At low frequencies, this was found to be negligible. At high frequencies, it was possible to observe flow behavior before the information arrived at the inlet, avoiding the issue altogether.

This case has the advantage of having an exact solution for truly incompressible flows. The solutions show that at a given time step, the pressure is linear in space while the velocity is constant. The exact solution is presented without derivation below.

$$u(t) = -\frac{\epsilon}{\rho_\infty u_\infty(1+\Omega^2)}\left[sin(wt) - \Omega cos(wt) + \Omega e^{-u_\infty t/L}\right] \tag{36}$$

$$p(x,t) = \left[\epsilon sin(wt) + \rho_\infty u_\infty u(t)\right]\frac{x}{L} - \rho_\infty u_\infty u(t) \tag{37}$$

When frequency and Mach number are low, the incompressible solution should be a good approximation of the compressible solution. Figs. 8 and 9 show this situation for both CUSP and matrix dissipation. Pressure (at the center of the domain) and velocity are plotted over time. Good agreement is shown between the exact incompressible solution for all methods, again validating the algorithms. Figs. 8c and 9c reiterate that the unsteady preconditioner is clearly preferred for convergence characteristics.

To understand the flow behavior as frequency increases, it is necessary to explore how the acoustic wave travel in time and space. The period of the outflow pressure oscillation ($T_w$) in seconds can be calculated by:

$$T_w = \frac{2\pi}{w} = \frac{2\pi L}{\Omega M_\infty c_\infty} \tag{38}$$

These pressure waves travel in space at the acoustic speed ($c$). Multiplying the period by the speed at which the wave travels, yields the physical period ($L_w$) of the sinusoidal pressure wave.

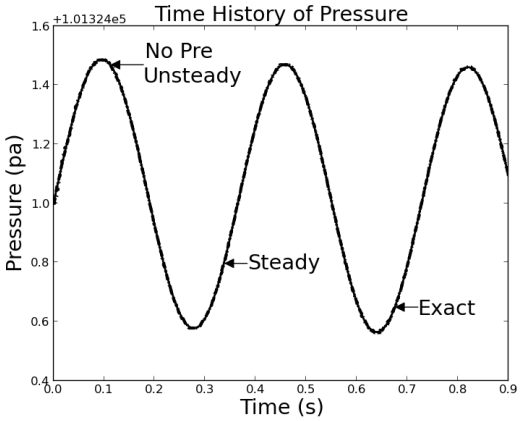


**a) Pressure over time (at center).**

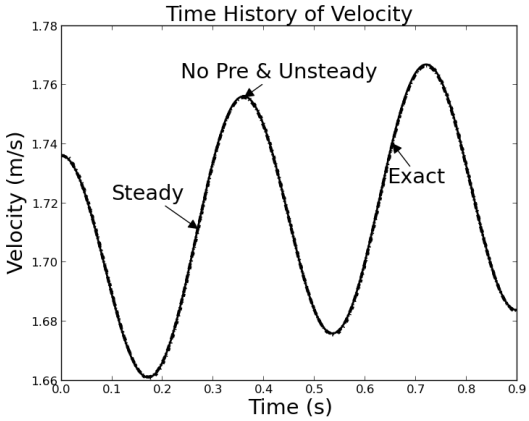


**b) Velocity over time.**

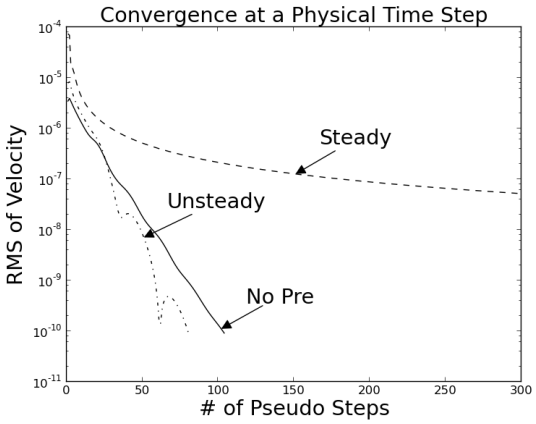


**c) Convergence**

**Figure 8. Plots of oscillating back pressure with matrix diffusion using a 2D mesh of 128 by 4 with a $CFL_c = 100$, $Str = 81.5$, $Mach = 0.005$, $\Omega = 10$.**

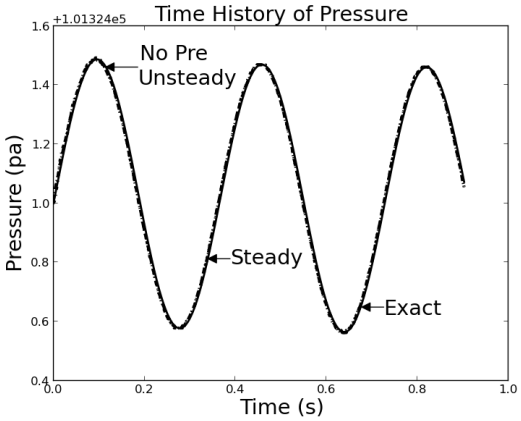


**a) Pressure over time (at center).**

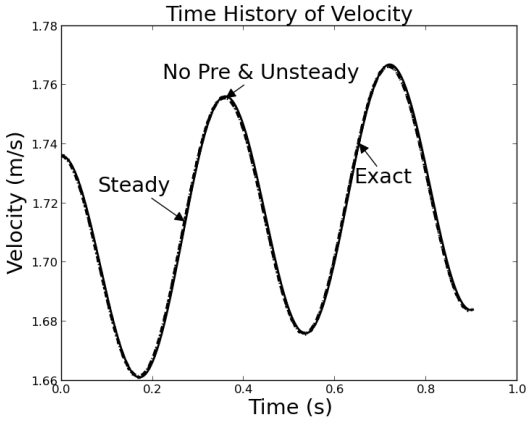


**b) Velocity over time.**

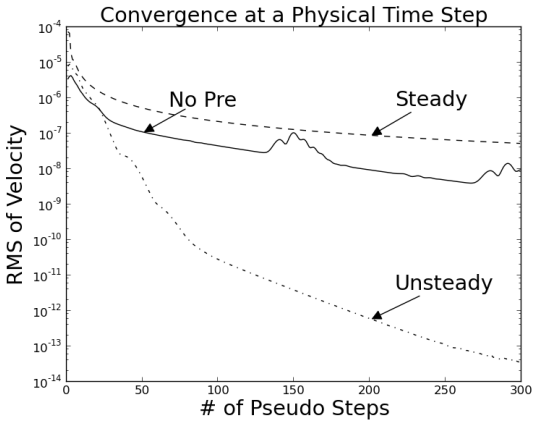


**c) Convergence**

**Figure 9. Plots of oscillating back pressure with CUSP diffusion using a 2D mesh of 128 by 4 with a $CFL_c = 100$, $Str = 81.5$, $Mach = 0.005$, $\Omega = 10$.**

$$L_w = c_\infty T_w = \frac{2\pi L}{\Omega M_\infty} \tag{39}$$

When frequencies are low (i.e. $\Omega = 10$) the physical period of the wave is much larger than the domain of the problem. In these cases, the pressure will appear linear and the incompressible exact solution becomes a good approximation. $L_w$ in Figs. 8 and 9 was approximately 125 times larger than the domain length. As $\Omega$ increases the solution becomes increasingly invalid. Fig. 10 shows a case where $\Omega = 100$. Here, the physical period is about 12.5 times larger than the domain scale. The curvature of the physically acoustic waves is now no longer negligible. Fig. 10a shows the pressures at the center of the domain. It is clear that the compressible effect of the pressure waves is beginning to manifest in the solution.

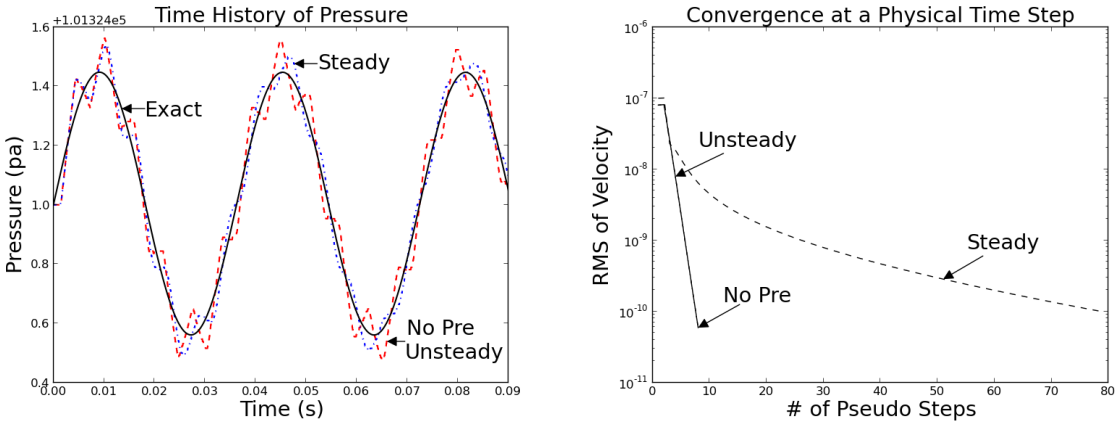


**a) Pressure over time (at center).** **b) Convergence**

**Figure 10. Plots of oscillating back pressure with matrix diffusion using a 2D mesh of 128 by 4 with a $CFL_c = 1$, $Str = 8150$, $Mach = 0.005$, $\Omega = 100$.**

To explore the effects of the acoustic waves over the domain of the pipe, $\Omega$ was increased to 4000. This creates a physical period about 1/3 the length of the domain. The expected solution over the domain is a perfectly traced sinusoidal pressure wave that correlates to the outflow oscillations. Figs. 11a and 12a show the pressure waves, as they are allowed to travel leftwards through the domain. In order to accurately track the high frequency waves, $CFL_C$ was reduced dramatically to 0.025.

Table 1 states that for a pressure driven problem, the steady state preconditioner should struggle when matrix dissipation is used. This is consistent with the wave portrayed in Fig. 11a. The addition of the modified CUSP scheme improves the steady state preconditioner accuracy in this regime.

Even though CUSP is able to improve the accuracy of the physical pressure waves using the steady preconditioner, the steady preconditioner convergence still suffers. This is highlighted in Figs. 11b and 12b. Unsteady preconditioning in combination with CUSP is capable of accurately capturing both velocity and pressure fields, and has better convergence characteristics.

## V. Conclusions and Future Work

A new convective-upwind split-pressure (CUSP) scheme was introduced this is suitable for unsteady flows in the low Mach number high Strouhal number regime. The new scheme follows closely the original CUSP scheme of Jameson, but with additional pressure diffusion to improve scaling and conditioning at low Mach numbers. The behavior of the preconditioned CUSP scheme was studied for acoustic dominated problems by setting up flow in a pipe with oscillating back-pressure. For convection-dominated flows, the scheme was evaluated for a propagating inviscid vortex. The new CUSP scheme significantly reduced discretization errors in both cases. It was also shown that the introduction of the Strouhal number into the preconditioning definition improves efficiency greatly as time steps become small. Combining the new CUSP with unsteady preconditioning is robust and improves accuracy as well as efficiency of compressible CFD algorithms for low speed flows.

Future work will focus on the linearization of the CUSP scheme for implicit schemes requiring Jacobian terms. All results is this work were obtained using matrix dissipation for the Jacobian terms regardless of the right-hand side

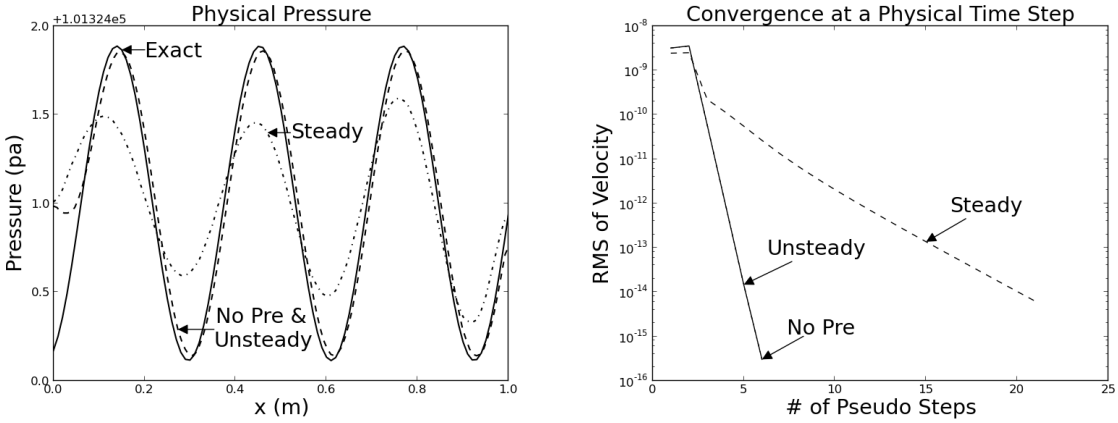


**a) Pressure over the domain.** **b) Convergence**

**Figure 11. Plots of oscillating back pressure with matrix diffusion using a 2D mesh of 128 by 4 with a $CFL_c = 0.025$, $Str = 326000$, $Mach = 0.005$, $\Omega = 4000$.**

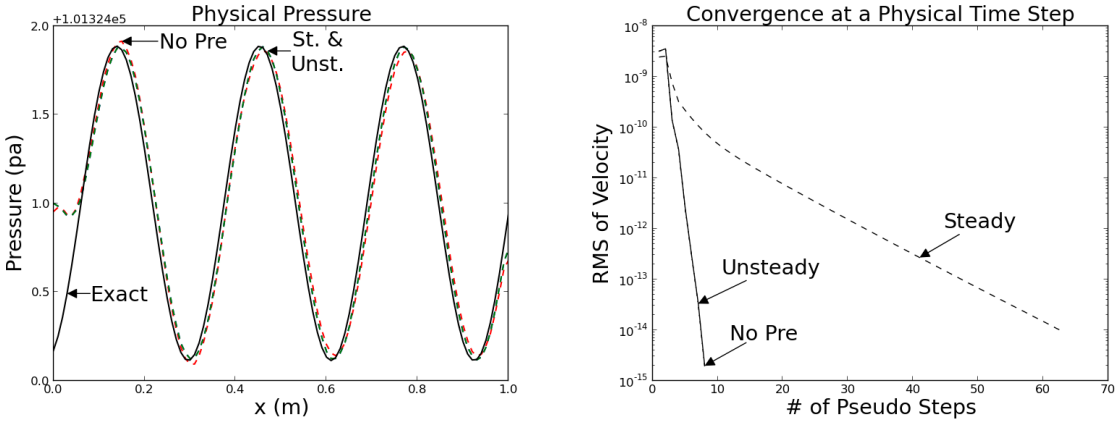


**a) Pressure over the domain.** **b) Convergence**

**Figure 12. Plots of oscillating back pressure with CUSP diffusion using a 2D mesh of 128 by 4 with a $CFL_c = 0.025$, $Str = 326000$, $Mach = 0.005$, $\Omega = 4000$.**

spatial discretization. This strategy was adopted to preserve diagonal dominance. However, a consistent left-hand side treatment would likely further improve convergence. Consistent and diagonally dominant linearization of the new scheme is an area of future research. In addition, future work will focus on defining the Strouhal number based on local flow conditions rather than as a global input, which requires some a priori knowledge of the problem. Local scaling could more effectively adapt the preconditioner and require less user input.

## References


[1] Venkateswaran, S. and Merkle, C. L., "Analysis of Preconditioning Methods for the Euler and Navier-Stokes Equations," Von karman institute lecture series, University of Tenesse Space Institute, Tullahoma, TN, 1999.

[2] Weiss, J. and Smith, W., "Preconditioning Applied to Variable and Constant Density Flows," *AIAA Journal*, Vol. 33, No. 11, November 1995, pp. 2050–2057.

[3] Turkel, E., "Preconditioning Techniques in Computational Fluid Dynamics," Annual Review 1999.31, Annu. Rev. Fluid Mech., 1999.

[4] Caughey, D. and Jameson, A., "Fast preconditioned multigrid solution of the Euler and NavierStokes equations for steady, compressible ows," *International Journal for Numerical Methods in Fluids*, Vol. 43, 2003, pp. 537–553.

[5] Charles L. Merkle, Jennifer Y. Sullivan, P. E. O. B. and Venkateswaran, S., "Computation of Flows with Arbitrary Equations of State," *AIAA Journal*, Vol. 36, No. 4, 1998, pp. 512–521.

[6] Xia, G., Sardeshmukh, S., Sankaran, V., and Merkle, C., "Implementation of an Enhanced Flux Formulation for Unsteady Navier-Stokes Solutions," Tech. rep., 4th International Conference on Computational Fluid Dynamics, Ghent, July 2006.

[7] Potsdam, M., Sankaran, V., and Pandya, S., "Unsteady Low Mach Preconditioning with Application to Rotorcraft Flows," *AIAA paper* 2007-4473, AIAA Computational Fluid Dynamics Conference, Orlando, FL, July 2007.

[8] Hosangadi, A., Sachdev, J., and Sankaran, V., "Improved Flux Formulations for Unsteady Low Mach Number Flows," Tech. Rep. ICCFD7-2202, 7th International Conference on Computational Fluid Dynamics, Big Island, Hawaii, July 2012.

[9] Liou, M. and Steffen, C., "A New Flux Splitting Scheme," *Journal of Computational Physics*, Vol. 107, 1993, pp. 23–39.

[10] Liou, M., "A Sequel to AUSM: AUSM$^+$," *Journal of Computational Physics*, Vol. 129, 1996, pp. 364–382.

[11] Liou, M., "A sequel to AUSM, Part II: AUSM$^+$-up for all speeds," *Journal of Computational Physics*, Vol. 214, 2006, pp. 137–170.

[12] Jameson, A., "Analysis and Design of Numerical Schemes for Gas Dynamics 1 Artificial Diffusion, Upwind Biasing, Limiters and Their Effect on Accuracy and Multigrid Convergence," *International Journal of Computational Fluid Dynamics*, Vol. 4, 1995, pp. 171–218.

[13] Jameson, A., "Analysis and Design of Numerical Schemes for Gas Dynamics 2 Artificial Diffusion and Discrete Shock Structure," *International Journal of Computational Fluid Dynamics*, Vol. 5, 1995, pp. 1–38.

[14] Zha, G., Shen, Y., and Wang, B., "An improved low diffusion E-CUSP upwind scheme," *Computers and Fluids*, Vol. 48, 2011, pp. 214–220.

[15] Shen, Y. and Zha, G., "Low diffusion E-CUSP scheme with implicit high order WENO scheme for preconditioned Navier-Stokes equations," *Computers and Fluids*, Vol. 55, 2012, pp. 13–23.